Nanoscale

Accepted Manuscript

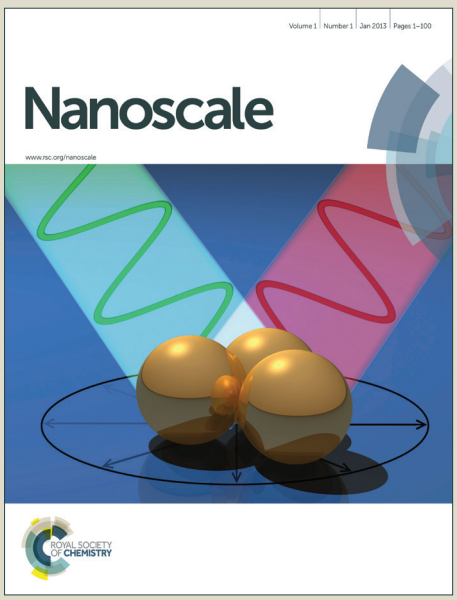

ROYAL SOCIETY OF CHEMISTRY

www.rsc.org/nanoscale

Carbon with ultrahigh capacitance when graphene paper meets $K_3Fe(CN)_6$

Kunfeng Chen[1], Fei Liu[1], Dongfeng Xue[1,] and Sridhar Komarneni[2,*]*

[1]State Key Laboratory of Rare Earth Resource Utilization, Changchun Institute of Applied Chemistry, Chinese Academy of Sciences, Changchun 130022, China

[2]Materials Research Institute, Materials Research Laboratory, The Pennsylvania State University, University Park, Pennsylvania, 16802, United States

*E-mail: dongfeng@ciac.ac.cn; komarneni@psu.edu

For the first time, we showed a novel supercapacitor system with graphene paper electrode in the redox-electrolyte of $K_3Fe(CN)_6$ based on the system-level design principle. By combining electric double-layer capacitance and pseudocapacitance, the specific capacitance could be increased 5-fold compared with the conventional electrode-electrolyte system. This large improvement is attributed to the additional redox reactions to the graphene paper electrode via the constituent ions of $K_3Fe(CN)_6$ in redox-electrolyte, during which the discharge process is highly enhanced. More importantly, the potential interval could reach as high as 1.6 V beyond the limited operating voltage of water (~1.23 V). After 5000 continuous cycles, 94 % of the initial capacitance was retained. The currently designed novel supercapacitor system is binder-free, conducting additive-free and can deliver higher capacitance. This designed graphene-paper-electrode/redox-electrolyte system can provide a versatile strategy for high-capacitance supercapacitor systems.

Keywords: graphene paper, supercapacitor system, redox-electrolyte, $K_3Fe(CN)_6$, pseudocapacitance

As the global demand for energy and the concerns of environmental pollution grow, clean renewable energies become appealing to replace the conventional energy platform based on fossil fuels. [1-3] Electrochemical energy storage technologies, including lithium-ion batteries, supercapacitors and redox flow batteries, are the most promising for the future energy needs. [1,2] Supercapacitors fall between rechargeable batteries and capacitors, which can offer higher power with fast charge/discharge rates and a much longer cycle life than rechargeable batteries, but have lower amount of energy than batteries. [4-6] The amount of electrical energy (E) accumulated in a capacitor is related to the capacitance (C) and voltage (V) according to the formula: $E=0.5CV^2$. Therefore, the improvement in energy of a supercapacitor can be achieved by either maximizing the specific capacitance and/or the cell voltage.[7] Many efforts have been made to improve the energy density of supercapacitors on the basis of designing high-performance electrode materials, for example, porous and/or nanosized electrode materials with large surface area were developed to enhance the specific capacitance. [4,7-9] Recently, system-level design of the theoretical and experimental efforts is becoming increasingly important for the development of modern materials science,[10] and the design of high-performance supercapacitors system requires both positive and negative electrodes to be precisely coupled with an electrolyte. However, hybrid supercapacitors typically showed enhanced energy density at the expense of power performance because the redox reaction of battery electrode occurred within the crystalline framework of active materials.[7] Furthermore, the coupled electrode/electrolyte system was designed and fabricated to include carbon electrode and redox-electrolyte with the combination of two charge-storage mechanisms: electric double-layer capacitance and Faradaic pseudocapacitance.[11-13]

Graphene-based supercapacitors have been receiving much attention due to their unique structures and electronic properties,[14-16] and the superior electron mobility of graphene can facilitate the electron propagation during the charge/discharge processes.[17-19] The theoretical maximum gravimetric specific double-layer capacitance of graphene electrode was calculated

to be ~ 550 F/g. [15] When used as electrode for a supercapacitor, graphene paper without using blending conductive additives and binders, could show significantly improved performance compared to other available carbon materials. [20,21] Recently, a flexible, all-solid-state laser-scribed graphene electrochemical capacitor (LSG-EC) was fabricated and the areal capacitance of the LSG-EC was calculated to be 3.67 mF/cm^2 (and 4.04 mF/cm^2 in 1.0 M H_2SO_4) at 1A/g $_{LSG/electrode}$. [16] Folded structured graphene paper supercapacitors gave the specific capacitance up to 172 F/g at the charge/discharge rate of 1 A/g, and the capacitance of 110 F/g was obtained even when the supercapacitor was operated at the fast rate of 100 A/g. [22] Although these binder-free electrodes afford increased capacity, their energy storage properties are generally attributed to electric double-layer capacitance, which limits further increase in capacitance.

In order to improve the specific capacitance of graphene paper supercapacitors, we designed graphene-electrode/redox-electrolyte supercapacitor system with the combination of Faradaic pseudocapacitance and electric double-layer capacitance. A water-soluble redox couple $Fe(CN)_6^{3-}/Fe(CN)_6^{4-}$ was selected as the redox-electrolyte due to its low toxicity coupled with high stability, and wildly adopted for study on electrode characterization.[23-27] In alkaline aqueous electrolyte, redox couple $Fe(CN)_6^{3-}/Fe(CN)_6^{4-}$ has been used as the cathode, which can carry out the charge storage.[23] The enhancement of pseudocapacitance through both $Co(OH)_2$/graphene nanosheets electrode and $K_3Fe(CN)_6$ electrolyte was previously reported.[26] This electrode system showed an ultrahigh specific capacitance of 7514 F/g at 16 A/g in mixed 1 M KOH and 0.08 M $K_3Fe(CN)_6$ electrolyte. The improvement on the capacitive properties of Co-Al layered double hydroxide by adding $K_3Fe(CN)_6$ or $K_4Fe(CN)_6$ to 1M KOH was also reported.[27] In these cases, both the electrode materials and electrolyte showed pseudocapacitance character and the used electrolyte was alkaline KOH solution. In this work, electrode materials with electric double-layer capacitance were studied in neutral $K_3Fe(CN)_6$ solution. However, most specific capacitances were only calculated according to

the weight of electrode materials. Because the actual specific capacitance in redox-electrolyte originates from both electrode and redox-electrolyte, the value of areal capacitance can reflect the actual capacitance contribution in redox-electrolyte system.

Herein, graphene-paper/redox-electrolyte supercapacitor system was designed by system-level planning of electrode and electrolyte, which has a binder-free, conducting additive-free electrode and can deliver very high capacitance. With the use of calculated areal capacitance, the real capacitance contribution from both electrode and electrolyte was identified. With the introduction of redox-electrolyte of $K_3Fe(CN)_6$ into Na_2SO_4 electrolytes, we obtained a 5-fold increase in the specific capacitances compared with that in only Na_2SO_4 electrolyte. The $[Fe(CN)_6]^{3-}$ ions in redox-electrolyte provided additional redox pseudocapacitance to the graphene paper electrode, which enhanced its specific capacitance. This graphene-paper-electrode/redox-electrolyte system is a versatile strategy to design high-capacitance supercapacitors.

The graphene-paper-electrode/redox-electrolyte supercapacitor system was designed to demonstrate a versatile way for the fabrication of the high-performance supercapacitor system. Scheme 1 shows the charge storage mechanism of a graphene paper electrode in a traditional electrolyte and a redox-electrolyte. In traditional Na_2SO_4 electrolyte, the specific capacitance of graphene electrode mainly comes from the electric double-layer capacitive behavior (Scheme 1a). CV curve shows a distinctive oxidation peak. When the as-formed graphene paper was tested in Na_2SO_4 electrolyte, electrochemical oxidation reaction can occur on graphene sheets as shown in the following equation: $>C + H^+ \rightarrow e^- + >COH, >CO, >COOH$. Thus, oxygen functional groups can be formed in-situ at the surface of graphene sheets. These oxidation reactions can produce oxidation peak on CV curves. However, these oxygen functional groups cannot be reduced and thus no reduction peaks can be found in CV curves.[18] After undergoing the initial electrochemical reaction in Na_2SO_4-$K_3Fe(CN)_6$

electrolyte, partial $[Fe(CN)_6]^{3-}$ ions were reduced to $[Fe(CN)_6]^{4-}$ and the redox couple of $[Fe(CN)_6]^{3-}/[Fe(CN)_6]^{4-}$ was formed. Therefore, additional pseudocapacitance could be easily generated from the redox reaction between $[Fe(CN)_6]^{3-}$ and $[Fe(CN)_6]^{4-}$ (Scheme 1b). The supercapacitor based on the system design of electrode and electrolyte has additional advantages (Figure S1): (1) in electrode aspect, the use of graphene paper can avoid the use of binder and conducting additives; (2) in electrolyte aspect, the use of redox-electrolyte can significantly increase specific capacitance values. The novel electrode and electrolyte system designed here can significantly increase the capacitance of supercapacitor due to the combined effect of pseudocapacitance and electric double-layer capacitance.

Graphene paper was obtained by mechanically pressing graphene aerogel. Graphene aerogel was synthesized by thermally reducing graphene oxide aerogel that was formed by freeze-drying route.[22,28] Figure 1a shows the scanning electron microscope (SEM) images of the as-synthesized graphene paper. These thin layers of graphene sheets stacked together to form 3D macrostructures, which favor the formation of the flexible self-supported graphene paper. The thickness of graphene paper was about 10 μm and an electronic conductivity of 18 S cm^{-1} was obtained. X-ray diffraction (XRD) pattern of graphene paper is shown in Figure 1b. The broad peak centered at $2\theta = 23.4°$ corresponds to the stacked graphene layers, which is mainly due to the existence of π–π stacking between graphene sheets.[29] The graphene paper with self-supported structure and high conductivity can be a good candidate for electrode in our designed supercapacitor system.

To validate the effect of redox-electrolyte on the enhanced capacitance, we studied the electrochemical performances of graphene paper in Na_2SO_4-$K_3Fe(CN)_6$ electrolyte. The specific capacitance as a function of the current density and charge/discharge curves are shown in Figure 2a-2c. The areal capacitances were calculated with equation (1) using the integral of the areas of the discharge curves in Figure 2b.

$$S_c = \frac{2I \cdot \int V dt}{A \cdot \Delta V^2} \quad (1)$$

where I(A) is the current used for charge/discharge, Δt(s) is the discharge time, A (cm^2) is the area of the graphene paper, and ΔV is the voltage interval. Specific areal capacitance values of 475, 240, 153, 105, and 76 mF/cm^2 were obtained from the discharge curves at various current densities of 20, 30, 40, 50 and 60 mA/cm^2 (Figure 2a). The capacitances decreased with the increase of current density, due to the existence of charge transfer polarization and concentration (mass transport) polarization. When the current density was as high as150 mA/cm^2, a specific area capacitance of 12 mF/cm^2 was obtained, which is much higher than the values reported previously. For example, the areal capacitance of the laser-scribed graphene electrochemical capacitors was calculated to be 3.67 mF/cm^2 at 1A/g $_{LSG/electrode}$.[16] Figure 2b, 2c and S2a show the galvanostatic charge/discharge curves with current density ranging from 20 to 150 mA/cm^2. The non-linear charge/discharge curves indicated the presence of pseudocapacitance. Figure S2b shows the energy density of graphene paper in Na_2SO_4-$K_3Fe(CN)_6$ electrolyte versus various current densities. The energy density of 169 $\mu Wh/cm^2$ was obtained at the current density of 20 mA/cm^2. The high specific capacitance and high potential range can produce the higher energy density.

Furthermore, CV curves were used to confirm the storage mechanism of electrochemical reaction. As shown in Figure 2d, a quasi-rectangular capacitive curve with the redox peaks at 0.18 and 0.35 V was observed, indicating that the involved capacitance includes both electric double-layer capacitance and pseudocapacitance. The electric charge storage mechanism of redox-electrolyte can be described by the following equation:

$$[Fe(CN)_6]^{3-} + e^- \leftrightarrow [Fe(CN)_6]^{4-} \quad (2)$$

A pair of reversible redox peaks can be observed in CV curves, where the oxidation peak is related to the charging process of $[Fe(CN)_6]^{4-}$ to $[Fe(CN)_6]^{3-}$ while the reduced peak is from the reverse process. The $[Fe(CN)_6]^{3-}$/$[Fe(CN)_6]^{4-}$ redox couple directly gives a

pseudocapacitance contribution to the graphene paper electrode, while graphene in traditional electrolyte has only electric double-layer capacitance. With the increase of scan rates, the oxidation and reduction peak potentials showed little change while the intensity of redox peaks increased leading to a high electrochemical activity and good charge/discharge reversibility. The graphene-$K_3Fe(CN)_6$ supercapacitors are excellent electron conductors with small equivalent series resistance demonstrated by the minimal change in shape of the CV curves as the scan rate increases from 5 to 60 mV/s.

In this graphene-$K_3Fe(CN)_6$ system, the actual capacitance was contributed by both electrode materials (graphene) and electrolyte ($K_3Fe(CN)_6$). In order to give the capacitance in F/g, we must know the weight of graphene and $K_3Fe(CN)_6$. However, not all $K_3Fe(CN)_6$ in electrolyte participated in the Faradaic reaction. Therefore, the weight of $K_3Fe(CN)_6$ electrolyte used in Faradaic reaction cannot be measured. The capacitance in F/g calculated from the only weight of graphene cannot evaluate the actual specific capacitance of this supercapacitor system. Because the pseudocapacitive reaction (2) occurred at the surface of electrode, the capacitance in F/cm^2 can reflect the real capacitance of this supercapacitor system, which is from the contribution of both electrode materials and electrolyte. Theoretical specific capacitance of $[Fe(CN)_6]^{3-}/[Fe(CN)_6]^{4-}$ redox reaction is 283.6 F/g calculated from equation $C_m = Q/(V \times M)$, where $Q = 9.632 \times 10^4$ C for the transfer of one electron during the redox reaction, M is molecular weight of $[Fe(CN)_6]^{3-}$ ion (M = 212.25 g/mol), V is the operating potential window (1.6 V). It is obvious that these redox-electrolyte ions can effectively increase the electrochemical performance of the current carbon-based materials.

Figure 2e shows the dependence of the anode peak current I_p on scan rate v. The best fit of the data to an apparent power-law dependence yields $I_p \propto v^{0.53}$. The current response to an applied scan rate will vary depending on whether the redox reaction is diffusion-controlled or

surface controlled (capacitive).[6,30] The general relationship between peak current and scan rate can be written as follows:

$$I_p = C_1 v + C_2 v^{0.5} \quad (3)$$

For a diffusion-controlled reaction, $I_p \propto v^{0.5}$, while $I_p \propto v$ represents surface controlled reaction. Therefore, in Na_2SO_4-$K_3Fe(CN)_6$ electrolyte, the electrochemical reaction of graphene paper electrode is diffusion-controlled ($I_p \propto v^{0.53}$). Figure S3 shows CV curves and the peak current of graphene paper electrode in Na_2SO_4 electrolyte at various scan rates. The best fit of the data to an apparent power-law dependence yields $I_p \propto v^{0.81}$, which suggests that charge storage mechanism of graphene paper is mainly electric double layer capacitance (surface reaction control). These results showed that with the introduction of redox $K_3Fe(CN)_6$ electrolyte, the reaction mechanism of graphene paper electrode was changed from surface controlled to diffusion-controlled reaction.

To further evaluate the electrochemical properties of graphene-$K_3Fe(CN)_6$ supercapacitors, cycling stability of graphene paper electrode in $K_3Fe(CN)_6$-Na_2SO_4 electrolyte was tested. Figure 2f shows cycling performance of graphene paper electrode measured at the current density of 30 mA/cm^2. The initial electrolyte only includes $[Fe(CN)_6]^{3-}$ ions. After the initial electrochemical reaction, $[Fe(CN)_6]^{3-}$ was reduced to $[Fe(CN)_6]^{4-}$, and the redox couple of $[Fe(CN)_6]^{3-}$/$[Fe(CN)_6]^{4-}$ was obtained, which contributes additional capacitance to graphene paper electrode. However, the more $[Fe(CN)_6]^{3-}$/$[Fe(CN)_6]^{4-}$ ions are adsorbed on the graphene electrode surface, the larger is the resistance to Na^+ or SO_4^{2-} diffusion. Therefore, the specific capacitance was decreased until 1000 continuous cycles. With the increase of the cycling number, more $[Fe(CN)_6]^{3-}$ ions were reduced into $[Fe(CN)_6]^{4-}$ ions, and more $[Fe(CN)_6]^{3-}$/$[Fe(CN)_6]^{4-}$ ions were formed. With the increase of redox active compounds, the specific capacitance was increased from 1000 to 4500 cycles. The fluctuation in specific capacitance was due to the competition between

diffusion effect and redox power of $[Fe(CN)_6]^{3-}/[Fe(CN)_6]^{4-}$ ions. After 5000 continuous cycles, 94 % retention can be obtained compared with the initial value. The superior electrochemical performance of graphene-paper electrodes in $K_3Fe(CN)_6$ electrolyte can be explained by the following factors: (1) additional pseudocapacitance contribution from $Fe(CN)_6^{3-}/Fe(CN)_6^{4-}$ couple, (2) high conductivity of supercapacitor making electron and ion transfer more efficient and (3) no negative contribution from binder because it is binder-free.

To study the effect of $[Fe(CN)_6]^{3-}/[Fe(CN)_6]^{4-}$ on the electrochemical performances of graphene paper electrodes, we compared the CV and charge-discharge curves of graphene paper electrodes in Na_2SO_4 electrolyte and Na_2SO_4-$K_3Fe(CN)_6$ electrolyte. As shown in Figure 3a and S3a, the graphene paper electrode in only Na_2SO_4 electrolyte exhibited a quasi-rectangular CV curve. The linear galvanostatic charge and discharge curves can be observed in Figure 3b and 3c. These results indicated that the electric double-layer capacitance is the main charge storage mechanism of graphene paper in only Na_2SO_4 electrolyte. The specific areal capacitance value of 93 mF/cm^2 was obtained from the discharge curves at the current density of 20 mA/cm^2. The capacitance in 0.3 M $K_3Fe(CN)_6$ is ~5 times greater than that obtained in the absence of $K_3Fe(CN)_6$ (i.e., 475 mA/cm^2 compared to 93 mF/cm^2). The results proved that the pseudocapacitance of graphene paper electrodes was originated from the redox reaction of $[Fe(CN)_6]^{3-}/[Fe(CN)_6]^{4-}$.

To shed light on whether the capacitance was concentration dependent, we studied the electrochemical performance of graphene paper electrodes in Na_2SO_4 electrolyte by adding different concentrations of $K_3Fe(CN)_6$. Figure 3a displays CV curves of graphene paper electrode in redox electrolyte at the scan rate of 5 mV/s and at the potential range of –0.8 - 0.8 V. By adding $K_3Fe(CN)_6$ into Na_2SO_4 electrolyte, a pair of distinct redox peaks can be observed (Figure 3a) even at lower concentrations of 0.05 M. These peaks originated from the $[Fe(CN)_6]^{3-}/[Fe(CN)_6]^{4-}$ redox couple. The additional Faradaic pseudocapacitance was

present in redox electrolyte. The supercapacitor using graphene paper electrode and $K_3Fe(CN)_6$ electrolyte, combines two charge storage mechanism, electric double-layer capacitance and Faradaic pseudocapacitance. The characteristic CV shape and peak potential were not significantly influenced with the increase of the concentration of $K_3Fe(CN)_6$ (Figure 3a), which suggests the same electrochemical reaction mechanism. The area of CV curves increased with increasing concentration of $K_3Fe(CN)_6$, indicating that the specific capacitance of graphene paper electrodes was enhanced by increasing the concentration of $K_3Fe(CN)_6$.

Non-linear charge/discharge curves were observed by adding $K_3Fe(CN)_6$ to Na_2SO_4 electrolyte, further proving the presence of new redox couples in the present Na_2SO_4-$K_3Fe(CN)_6$ electrolyte (Figure 3b and 3c). The specific capacitances calculated from the integral area of galvanostatic discharge curves using equation (1) are shown in Figure 3d. The specific capacitances were 118, 157, 282 and 475 mF/cm^2 at the current density of 20 mA/cm^2 with the addition of 0.05, 0.1, 0.2, and 0.3 M $K_3Fe(CN)_6$, respectively (Figure 3d). Therefore, the specific capacitance was found to be dependent on the concentration of $K_3Fe(CN)_6$.

The charge transfer resistance and reaction kinetics were also investigated by electrochemical impendence spectroscopy (EIS). Figure 4a shows Nyquist plot of the electrochemical impedance spectroscopy, including a semicircle and a straight line. The interfacial charge-transfer resistance was calculated from the span of the single semi-circle along real-axis from the high to low frequency region. The equivalent series resistance is the intersecting point with real-axis in the range of high frequency. The inset of Figure 4a shows that the lowest equivalent series resistance was present with 0.3 M $K_3Fe(CN)_6$ electrolyte. The lowest charge transfer resistance, as indicated by the diameter of semicircle, was also observed at 0.3 M $K_3Fe(CN)_6$ electrolyte. The results proved that the resistance of supercapacitors decreased by increasing the concentration of $K_3Fe(CN)_6$ electrolyte. Upon increasing the $K_3Fe(CN)_6$ concentration, more $[Fe(CN)_6]^{3-}$/$[Fe(CN)_6]^{4-}$ ions play the role of

"electron shuttle" in the charge/discharge processes.[24-27] The lower resistance can facilitate a fast ionic and electronic transfer to guarantee a high capacitive performance.

Figure 4b shows Bode phase angle plots vs. frequency. At 0.01Hz, the phase angle of graphene paper electrode in only Na_2SO_4 electrolyte is higher than that in Na_2SO_4-$K_3Fe(CN)_6$ electrolyte. The closer the phase angle approaches 90°, the better is the capacitor behavior of the device.[29,30] The results presented here confirmed that by adding $K_3Fe(CN)_6$ to Na_2SO_4 electrolyte, the reaction mechanism of graphene paper electrode approaches diffusion-controlled type, which is consistent with relationship between peak current and scan rate. Fig. 4a and 4d show the values of the real (C′) and imaginary (C′′) part of the capacitance vs. frequency. Capacitance C′ is calculated by using the equation of $C' = -1/(2\pi f Z'')$, while the capacitance $C'' = 1/(2\pi f Z)$, where f is the frequency in Hz and Z'' and Z' is the imaginary and real part of the impedance spectrum.[31,32] The low-frequency C′ value corresponds to the so called static capacitance. C'' corresponds to energy dissipation of the capacitor by IR-drop and an irreversible Faradic charge transfer process, which can lead to the hysteresis of the electrochemical processes. Both C′ and C′′ values of graphene paper electrode in higher concentration of $K_3Fe(CN)_6$ were larger than those in lower $K_3Fe(CN)_6$ concentration. The present results proved that redox $K_3Fe(CN)_6$ electrolyte can significantly increase the electrochemical performance of graphene paper, which is in good agreement with CV and galvanostatic charge–discharge tests.

In summary, we developed a novel supercapacitor system that includes graphene paper electrode and redox-electrolyte according to the system-level design principle, which combines two kinds of charge storage mechanisms: electric double-layer capacitance and pseudocapacitance. New $[Fe(CN)_6]^{3-}/[Fe(CN)_6]^{4-}$ redox couple was present in this supercapacitor system, which contributes to pseudocapacitance. In neutral electrolyte, we obtained capacitance values of 475 mF/cm^2 in 0.3M $K_3Fe(CN)_6$-1M Na_2SO_4 redox-electrolyte

and 93 mF/cm^2 in 1 M Na_2SO_4 electrolyte with the potential interval of 1.6 V and the current density of 20 mA/cm^2. This large improvement in capacitance was attributed to the additional redox reactions to the graphene paper electrode via the constituent ions of $K_3Fe(CN)_6$ redox-electrolyte. In addition, the potential interval can reach as high as 1.6 V beyond the limited operating voltage of water (~1.23 V). After 5000 continuous cycles, the capacitance stayed at 94 % of the initial value. The superior electrochemical performance of graphene-paper electrodes in $K_3Fe(CN)_6$ electrolyte can be explained by the following factors: (1) additional pseudocapacitance contribution from $Fe(CN)_6^{3-}/Fe(CN)_6^{4-}$ couple, (2) high conductivity of supercapacitor making electron and ion transfer more efficient and (3) no adverse effect from binder as the system is binder-free. The system's approach developed here is a versatile way to design high-capacitance supercapacitors.

Acknowledgements

Financial support from the National Natural Science Foundation of China (grant no. 51125009) and National Natural Science Foundation for Creative Research Group of China (grant no. 21221061), and Hundred Talents Program of Chinese Academy of Science is acknowledged.

References

1 A. Manthiram, Y. Fu, Y. Su, *J. Phys, Chem. Lett.*, 2013, **4**, 1295–1297.

2 Z. Yang, J. Zhang, M. Kintner-Meyer, X. Lu, D. Choi, J. P. Lemmon, J. Liu, *Chem. Rev.*, 2011, **111**, 3577–3613.

3 J. B. Goodenough, K. S. Park, *J. Am. Chem. Soc.*, 2013, **135**, 1167–1176.

4 P. Simon, Y. Gogotsi, *Nat. Mater.*, 2008, **7**, 845–854.

5 B. E. Conway, Electrochemical Supercapacitors: Scientific Fundamentals and Technological Applications; Kluwer-Academic: New York, 1999.

6 V. Augustyn, P. Simon, B. Dunn, *Energy Environ. Sci.*, 2014, **7**, 1597-1614.

7 P. Sharma, T. S. Bhatti, *Energy Convers. Manage.*, 2010, **51**, 2901–2912.

8 K. Chen, S. Song, K. Li, D. Xue, *CrystEngComm*, 2013, **15**, 10367-10373.

9 I. E. Rauda, V. Augustyn, B. Dunn, S. H. Tolbert, *Acc. Chem. Res.*, 2013, **46**, 1113-1124.

10 P. Yang, J. Tarascon, *Nat. Mater.*, 2012, **11**, 560–563.

11 S. Roldan, C. Blanco, M. Granda, R. Menéndez, R. Santamaría, *Angew. Chem. Int. Ed.*, 2011, **50**, 1699–1701.

12 S. T. Senthilkumar, R. K. Selvan, Y. S. Lee, J. S. Melo, *J. Mater. Chem. A*, 2013, **1**, 1086–1095.

13 S. Roldan, M. Granda, R. Menendez, R. Santamaria, C. Blanco, *J. Phys. Chem. C*, 2011, **115**, 17606–17611.

14 A. K. Geim, K. S. Novoselov, *Nat. Mater.*, 2007, **6**, 183–191.

15 M. D. Stoller, S. Park, Y. Zhu, J. An, R. S. Ruoff, *Nano. Lett.*, 2008, **8**, 3498-3502.

16 M. F. El-Kady, V. Strong, S. Dubin, R. B. Kaner, *Science*, 2012, **335**, 1326−1330.

17 T. Kim, G. Jung, S. Yoo, K. S. Suh, R. S. Ruoff, *ACS Nano.*, 2013, **7**, 6899–6905.

18 F. Liu, D. Xue, *Chem. Eur. J.*, 2013, **19**, 10716–10722.

19 M. D. Stoller, C. W. Magnuson, Y. Zhu, S. Murali, J. W. Suk, R. Piner, R. S. Ruoff, *Energy Environ. Sci.*, 2011, **4**, 4685−4689.

20 D. A. Dikin, S. Stankovich, E. J. Zimney, R. D. Piner, G. H. B. Dommett, G. Evmenenko, S. T. Nguyen, R. S. Ruoff, *Nature*, 2007, **448**, 457–460.

21 D. Li, M. B. Muller, S. Gilje, R. B. Kaner, G. G. Wallace, *Nat. Nanotechnol.*, 2008, **3**, 101–105.

22 F. Liu, S. Song, D. Xue, H. Zhang, *Adv. Mater.*, 2012, **24**, 1089–1094.

23 Y. Lu, J. B. Goodenough, Y. Kim, *J. Am. Chem. Soc.*, 2011, **133**, 5756–5759.

24 S. T. Senthilkumar, R. Kalai Selvan, J. S. Melo, *J. Mater. Chem. A*, 2013, **1**, 12386-12394.

25 K. Chen, S. Song, D. Xue, *RSC Adv.*, 2014, **4**, 23338-23343.

26 C. Zhao, W. Zheng, X. Wang, H. Zhang, X. Cui, H. Wang, *Sci. Rep.*, 2013, **3**, 2986

27 L. Su, X. Zhang, C. Mi, B. Gao, Y. Liu, *Phys. Chem. Chem. Phys.*, 2009, **11**, 2195-2202.

28 K. Chen, F. Liu, S. Song, D. Xue, *CrystEngComm*, 2014, **16**, 7771-7776.

29 K. Chen, D. Xue, *J. Colloid Interface Sci.* 2014, **436**, 41-46.

30 K. Zhu, Q. Wang, J. Kim, A. A. Pesaran, A. J. Frank, *J. Phys. Chem. C*, 2012, **116**, 11895-11899.

31 Y. Honda, T. Haramoto, M. Takeshige, H. Shiozaki, T. Kitamura, M. Ishikawa, *Electrochem. Solid State Lett.*, 2007, **10,** A106-A110.

32 T. Thomberg, A. Janes, E. Lust, *J. Electroanal. Chem.*, 2009, **630**, 55-62.

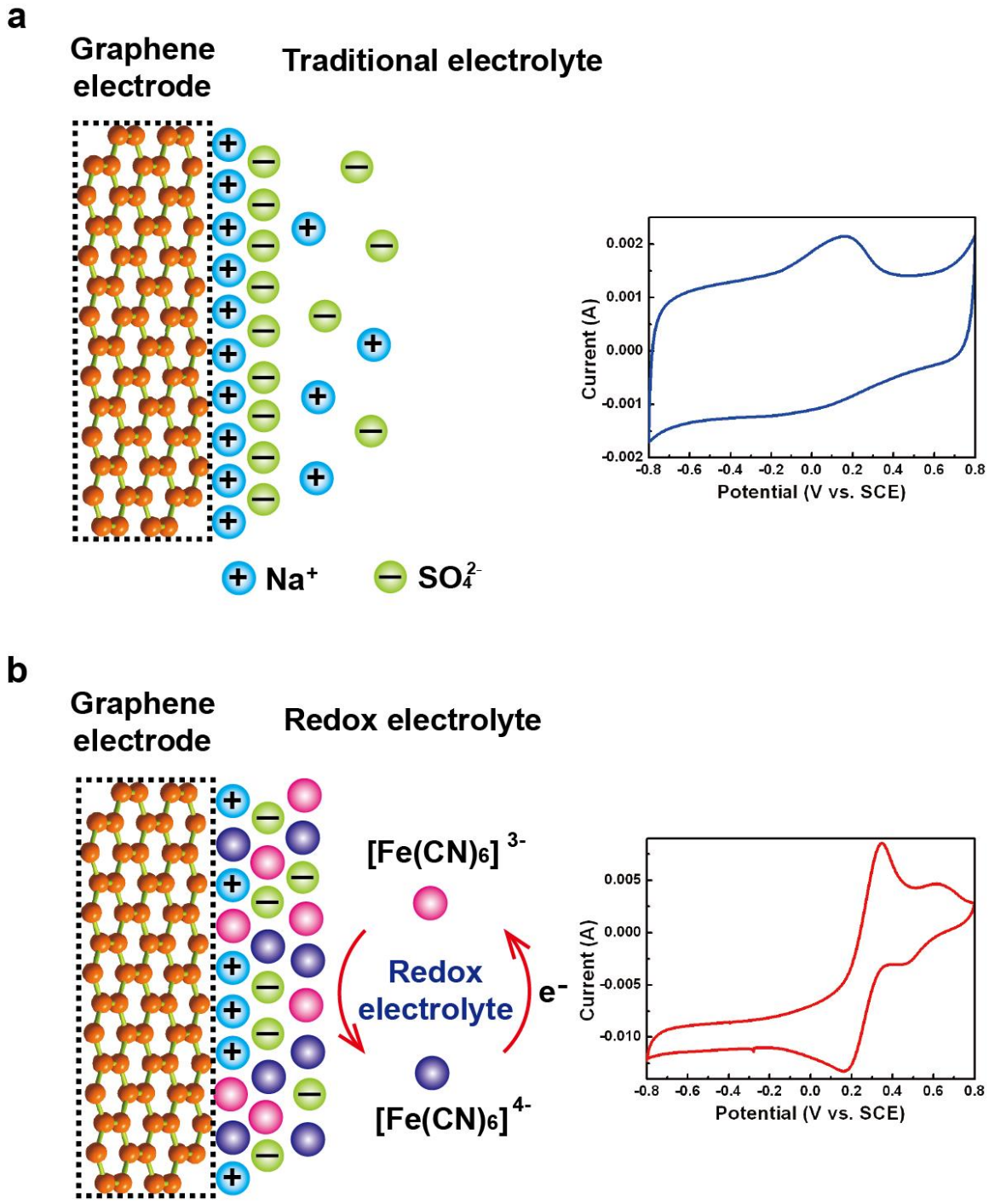

Scheme 1. Charge storage mechanisms of graphene paper electrode in the traditional electrolyte system (a) and the redox-electrolyte system (b). (a) Graphene paper electrode in neutral Na_2SO_4 electrolyte, which displays electric double-layer capacitance with quasi-rectangular CV curves. (b) After adding redox-active $K_3Fe(CN)_6$ to Na_2SO_4 electrolyte, this supercapacitor system combines two charge storage mechanisms, pseudocapacitance and electric double-layer capacitance. The novel electrode and electrolyte system can significantly increase the specific capacitance of supercapacitors.

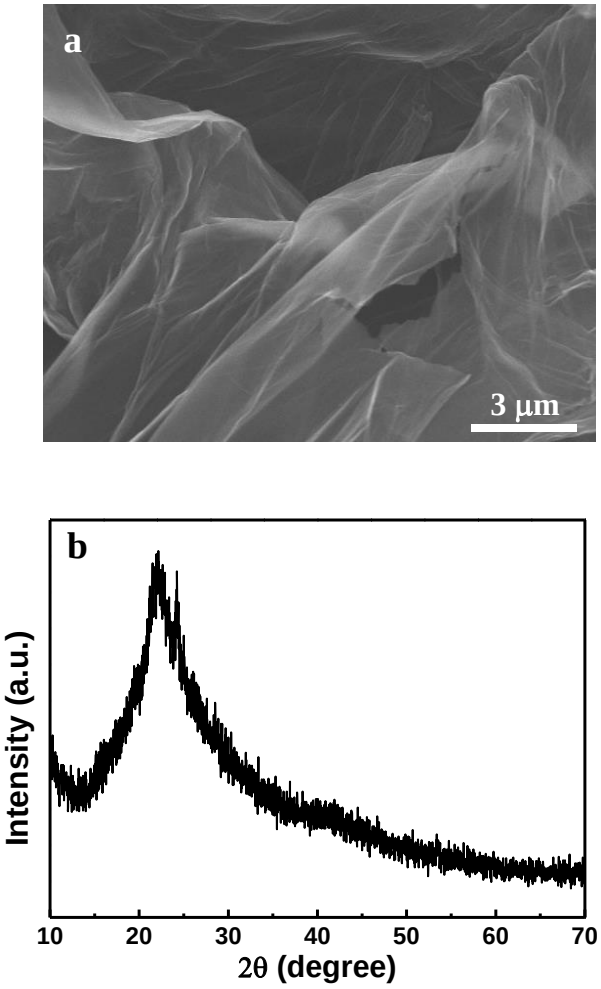

Fig. 1. SEM image (a) and XRD pattern (b) of the as-formed graphene paper. The thin layers of graphene sheets stacked together to form 3D macrostructures leading to self-supported structures.

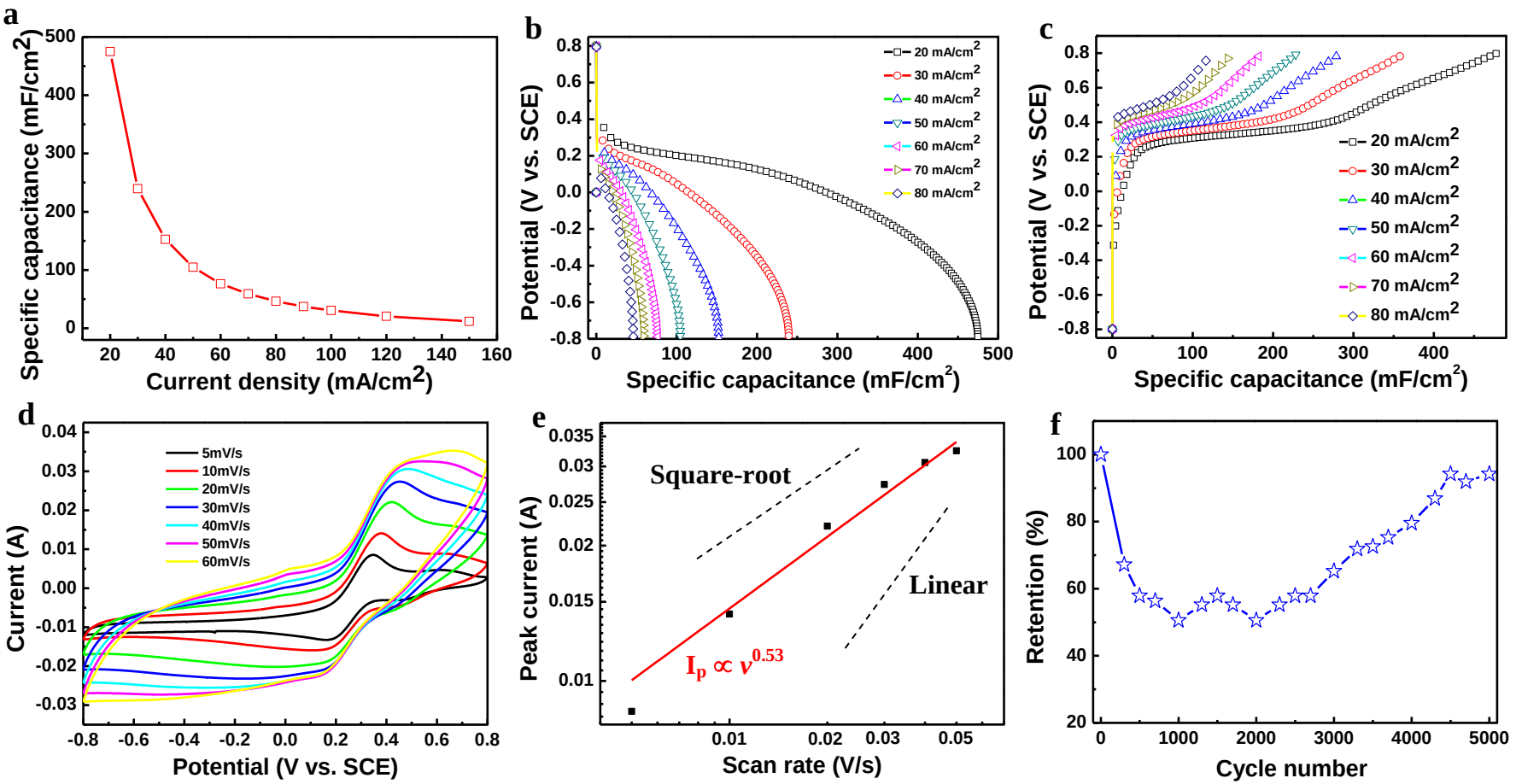

Fig. 2. Electrochemical performances of graphene paper electrode in redox-electrolytes including 1 M Na_2SO_4 and 0.3 M $K_3Fe(CN)_6$ solutions. (a) Specific areal capacitance as a function of current density. (b) The discharge and (c) charge curves measured at various current densities and the potential interval of 1.6 V. (d) CV curves (current density versus potential) at various scan rates and the potential range from –0.8 to 0.8 V. (e) The anode peak current at various scan rates. (f) Cycling stability of graphene paper electrode at the current density of 30 mA/cm^2.

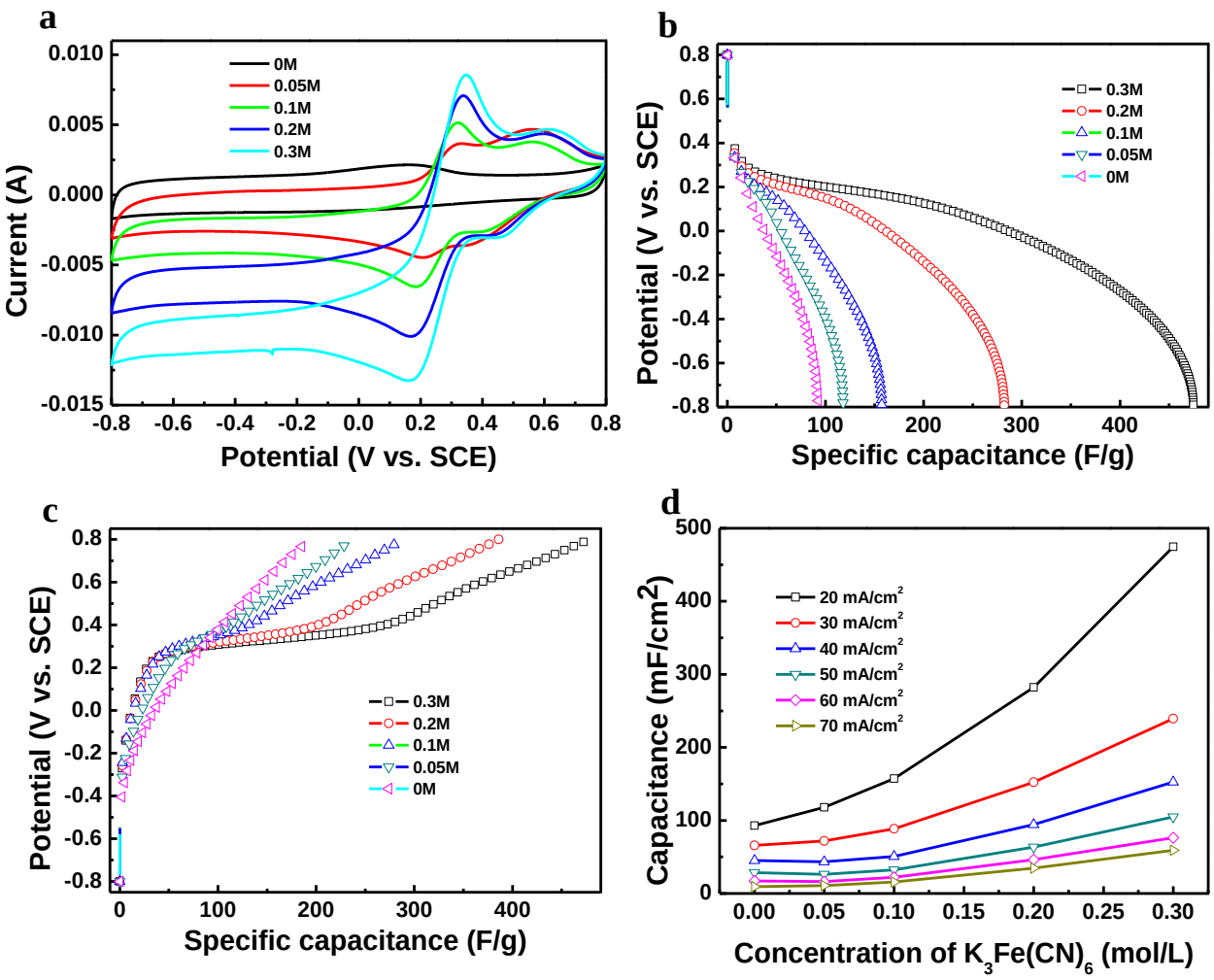

Fig. 3. Electrochemical performance of graphene paper electrodes in redox-electrolytes including 1M Na_2SO_4 and the different concentrations of $K_3Fe(CN)_6$ solutions (indicated in graph). (a) CV curves at the scan rate of 5 mV/s and the potential range from –0.8 to 0.8 V. A pair of redox peaks is present at the CV curves, showing the pseudocapacitive characteristic with the introduction of $K_3Fe(CN)_6$ into Na_2SO_4 electrolyte. The discharge (b) and charge (c) curves measured at the current density of 20 mA/cm^2 and the potential range from –0.8 to 0.8V. (d) Specific capacitance versus current density and the concentrations of $K_3Fe(CN)_6$.

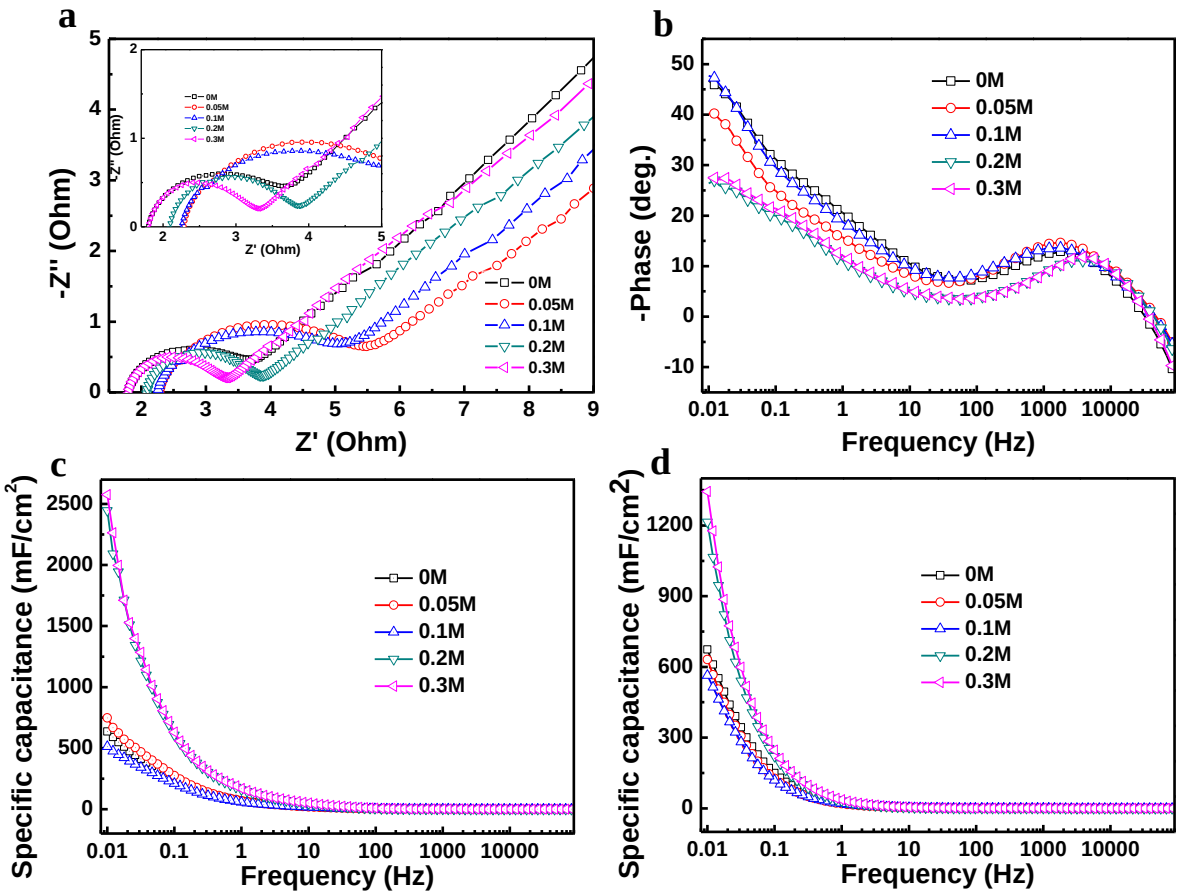

Fig. 4 Electrochemical impedance spectroscopy (EIS) of graphene paper electrode in redox-electrolytes including 1M Na_2SO_4 and the different concentrations of $K_3Fe(CN)_6$ solutions (indicated in graph). (a) Nyquist plots, (b) plots of impedance phase angle versus frequency, (c) and (d) plots of specific area capacitance versus frequency calculated from imaginary (c) and real part (d) of impedance spectroscopy. The inset in (a) shows Nyquist plots at high frequencies.

TOC

Novel supercapacitor system with graphene paper electrode in redox-electrolyte of $K_3Fe(CN)_6$ was designed by system-level planning of electrode/electrolyte systems.